The Ancillary Response of Storage Power Plants (SPP) in the Present and Future Electrical Grid

Prof. Dr.-Ing. Harald Weber
Electrical Energy Supply (EEV), Institute for Electrical Power Engineering (IEE)
University of Rostock, 18059 Rostock, Germany, harald.weber@uni-rostock.de

Abstract

It is expected that in the near future, the electrical power supply networks will be significantly revolutionized. Most of today's conventional power plant structures will give way to a novel, inertia independent (free from rotating masses) power plant system. Such systems, called storage power plants, will possess storages for different generation speed together with power electronic converters. They will be able to integrate and store energy from renewable sources. However, to be deemed truly feasible in the present scenario, these storage power plants must be able to function efficiently when they are integrated with conventional power plants and renewable energy sources. They should be able to satisfy the frequency dependent grid regulatory services involving spinning reserve, primary and secondary control in combination with other types of power plants. Hence, in this paper, the storage power plants are connected with thermal, hydroelectric and wind power plants, in a single network, and their dynamic ancillary response is studied when there are sudden disturbances in the electrical grid in the form of changes in power consumption by loads or generation from renewable sources.

1 Introduction

Presently, 14.8% of Germany's gross final energy consumption (around 2500 TWh) originates from renewable energy sources (RES)[1]. The aim of the EU 2020 energy strategy is to raise this share to 18% with future targets projecting it to be around 60% by the year 2050 [2, 3, 4]. Such high penetration of RES (primarily wind and solar), although necessary, introduces additional challenges in ensuring stability and reliability of the electrical grid. The ever increasing infeed from these RES leads to higher frequency fluctuations, presence of harmonics as well as increased forecast errors due to their intermittent nature [5].

The difference between the varying electrical energy generation from RES and consumption by loads leads to either an energy deficit or surplus in the grid. At present, conventional power plants (CPPs) have to compensate for this disparity. However, in the future, the number of these CPPs, especially coal fired power plants, will decrease drastically to fulfill energy sector targets [6]. Thus, Electrical Energy Storage (EES) systems are regarded as viable alternatives to compensate for the intermittent and decentralized RES, so that the network demand can be met at all times.

Depending on its principle an EES type has different advantages and disadvantages. Flywheels and supercapacitors have high charge and discharge rates, but, due to their sizes, are impractical long-term energy storages [7]. In comparison to supercapacitors, battery energy storages have a higher energy density, but a much slower response [8]. Meanwhile, hydrogen storages can be used to supply or store large magnitudes of energy but, due to the rate of the electrochemical reactions in a fuel cell or electrolyser, they have an even slower response. A combination of these elements, though, will not only compensate for the shortcomings of these individual storage types but also assist in exploiting their advantages. Hence, such an interconnected system is presented in this paper, called Storage Power Plant (SPP).

The operation of a SPP in an electrical grid with nodal voltage angle control as ancillary service has been discussed before [9, 10]. Then again, to be regarded as a suitable solution for the current situation, the SPP also needs to function coherently with CPPs and RES in a frequency governed grid. Hence, the goal of this paper is to show the dynamic interaction between these different types of power plants. The following section describes the electrical grid, which is used as the test environment for this study. This is followed by an explanation of the component chain present inside a SPP, focusing on the role of each element. The result section comprises of two parts where the response of these power plants is analyzed, firstly during a step increase in load demand and secondly a ramp in power generation from RES. Finally, the highlights of the investigations are summed up in the conclusion.

2 Test Electrical Network

The example network on which the investigations are carried out is shown in Fig. 1. The grid consists of 25 equidistant nodes, each connected to either a power plant or a load. The nodes are interconnected via transmission lines, each 250 km long and at a voltage level of 110 kV. The line impedances are equal in magnitude with a resistance to reactance ratio of 0.1.

There are eleven power plants, of which five are slack SPPs (*S*), i.e. converters at terminals where the voltage

ISBN 978-3-8007-5081-8

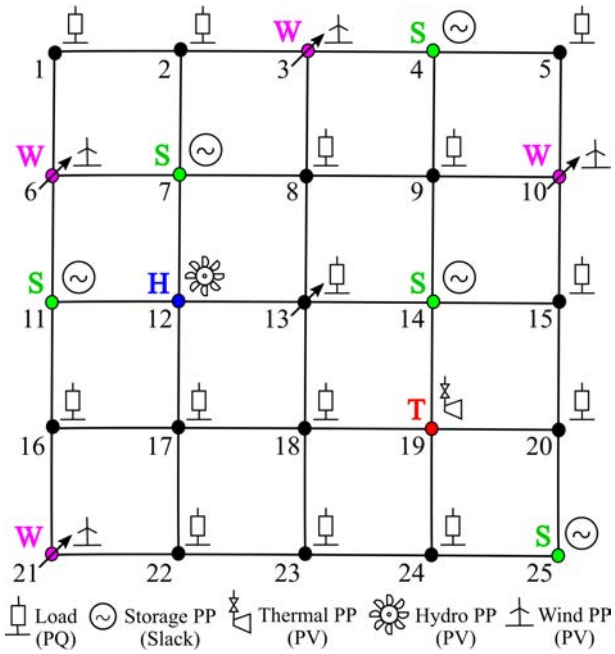

Figure 1 25 node example network

magnitude ($|V|$) and angle (ϕ_u) are kept constant. Out of the other six, four represent wind power plants (W), while the other two each denote a conventional hydroelectric (H) and a coal fired thermal (T) power plant. The CPPs are represented by PV terminals, where the active power (P) and voltage magnitude ($|V|$) are controlled. The four wind power plants (WPPs) and remaining 14 nodes, each housing a load, are represented by PQ terminals where the active (P) and reactive power (Q) being consumed are known. The network modeling and simulations are carried out in the software DIgSILENT PowerFactory. The base power value of the per-unit-system is 10 MVA. It is assumed that each of the 14 loads consumes 4 MW of active power. The total deficit of 56 MW is satisfied by the five storage, two conventional and four WPPs. The five SPPs and two CPPs each produce 5 MW, while the four WPPs each generate 5.25 MW. Such values are chosen to keep the initial working points of the different types of power plants close to each other. This makes it easier to compare their output responses when sudden disturbances occur in the grid. Each load also consumes 1 MVAR of reactive power which is supplied later by the power plants. Unfortunately, the reactive power results and control methods are not included in this paper due to space constraints.

3 Internal SPP Structure

As seen in Fig. 2, the SPP consists of three main storages; the supercapacitor, battery and hydrogen storage. These storages have different energy capacities and are responsible for providing inertial, primary and secondary control respectively. There are DC-DC converters between the storages which control the power flow between them. All components operate in DC mode. Hence, the power plant uses a DC-AC converter for grid connection. The SPP structure used in the software, models the control scheme of the DC-DC converters which govern the power flow between the SPP storage components. The components themselves are represented by simplified ideal models.

The first storage, i.e. the supercapacitor, is directly connected to the DC-AC grid converter. In case of a network disturbance, it immediately supplies inertial power to the grid or stores it from the grid. It can instantaneously charge and discharge with high power and additionally has an almost infinite lifetime because of its electrostatic storage principal. These properties make it ideal for its task of providing inertial control. Hence, its behavior is analogous to the rotating mass in a turbine shaft of a conventional thermal power plant (TPP).

The second storage, i.e. the battery, connected in parallel to the supercapacitor, supplies or stores primary control power, in order to compensate for the low power density of the supercapacitor. This process is controlled by the DC-DC converter between these two components. In contrast to a supercapacitor, the battery is optimally suited for the purpose to provide primary control power. This is due to its electrochemical energy storage principle which allows

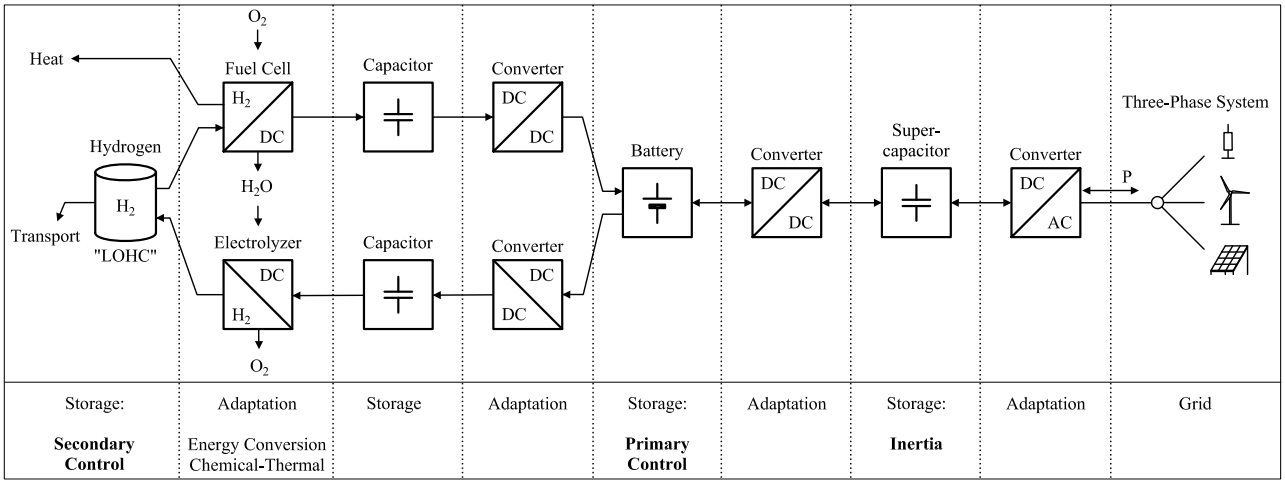

Figure 2 Working principle of the internal components of a storage power plant (SPP)

ISBN 978-3-8007-5081-8

it to possess a higher energy storage density and a preferably lower charging and discharging gradient, to improve its lifetime. Thereby, it represents the equivalent of the steam boiler in a conventional TPP.

As the third main storage, the hydrogen storage is responsible for supplying secondary control power, similar to the coal storage in a coal fired TPP. Additionally, it can store secondary control power. Depending on the power flow direction, either a fuel cell or an electrolyser is used to empty or refill the hydrogen storage. The power flow for each of these cases is controlled by the DC-DC converter in the respective paths between the hydrogen storage and the battery. Each of these two DC-DC converters possess a DC link buffer storage. The behavior of these capacitors is analogous to the steam boiler pipe wall in a TPP.

While utilizing the hydrogen storage, the fuel cell generates electrical energy from the chemical reaction between stored hydrogen (H_2) and external oxygen (O_2). One by-product of this reaction is thermal energy which can be used for district heating. Another product is dihydrogen monoxide (H_2O). In case of a reversed power flow, the H_2O can in turn be used as the electrolyte to generate hydrogen as well as oxygen as a by-product. The hydrogen can then be stored in a Liquid Organic Hydrogen Carrier (LOHC) system. Such a system enables safe, easy storage and transportation of hydrogen at a high energy density under ambient conditions, using the currently available infrastructure [11]. In addition to being used for electrical power generation in the SPP, the stored hydrogen can also be utilized for other applications, for example in automobiles.

4 Results and Observation

To analyze the dynamic behavior of the SPP in combination with the other power plants, two separate investigations are performed. In the first case, a step increase is applied to instantaneously raise the power consumption of the load at node 13 of the 25 node network. In the second case, the generation of all the WPPs are ramped by the equal magnitudes and the response of the power plants to the presence of surplus power in the grid is analyzed.

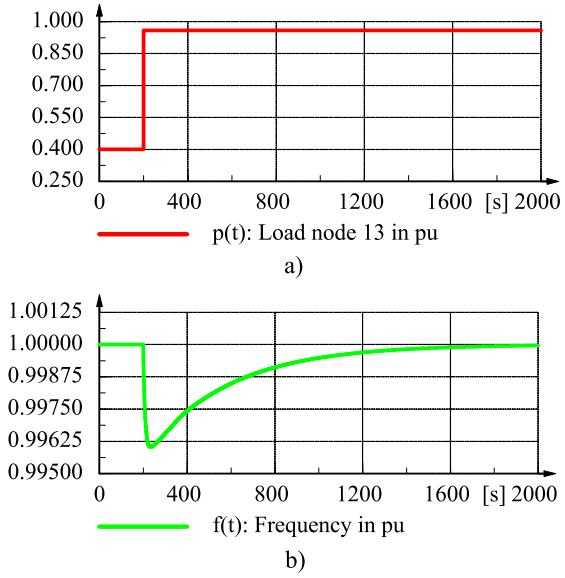

Figure 3 a) Step increase in the power consumption by the load at node 13 and b) Resulting change in frequency

4.1 Case I

The step increase applied at 200 s causes the power consumption by the load at node 13 to increase from 4 MW to 9.6 MW, shown as pu values in Fig. 3a. The magnitude of this increase is equal to 10% of the total power consumption (56 MW) in the network. In response, the grid frequency drops immediately at the inception of the load step, as shown in Fig. 3b. The rate of frequency change varies slightly for every node in the grid structure and is used by the respective power plants to provide their corresponding inertial response. The frequency deviation is used to provide primary control power and once the secondary control power starts to flow, the frequency is returned to 1 pu.

The ancillary response of the four different types of power plants to the increase in power demand at node 13 is shown in Fig. 4. In these investigations, since the WPPs are represented as converters operating at their constant rated power, they do not provide any ancillary service. Fig. 4a highlighting the inertial response of the different power plants exhibits that the SPP at node 7 immediately reaches its

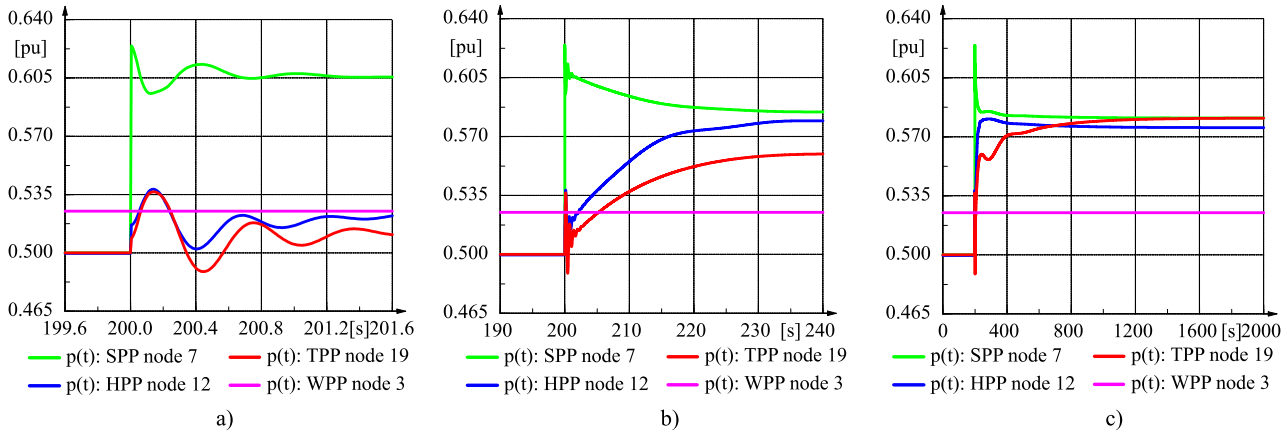

Figure 4 Response of the four different types of power plants due to the load step in increasing time frames

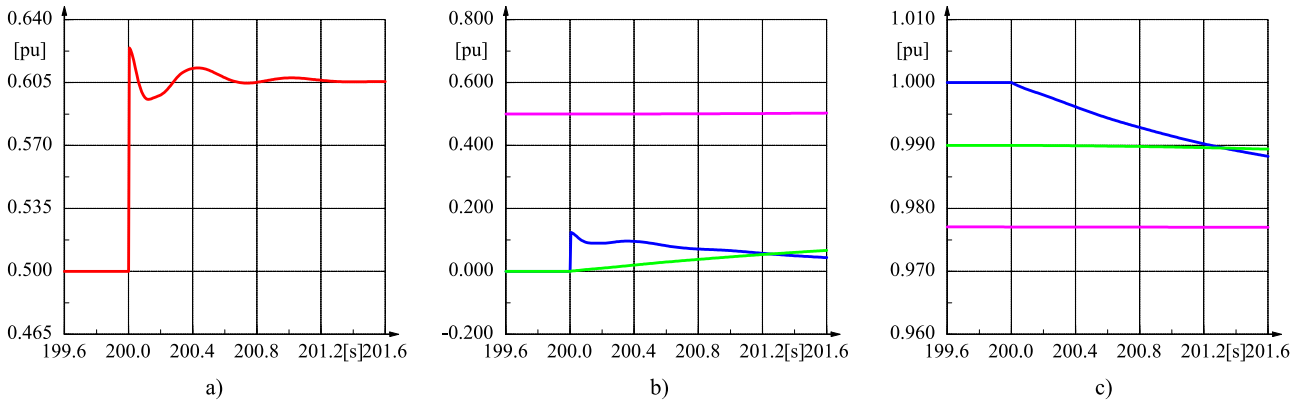

Figure 5 a) Increase in power output, b) Current flow from the SPP storages and c) Voltage levels of the storages during the initial short time frame

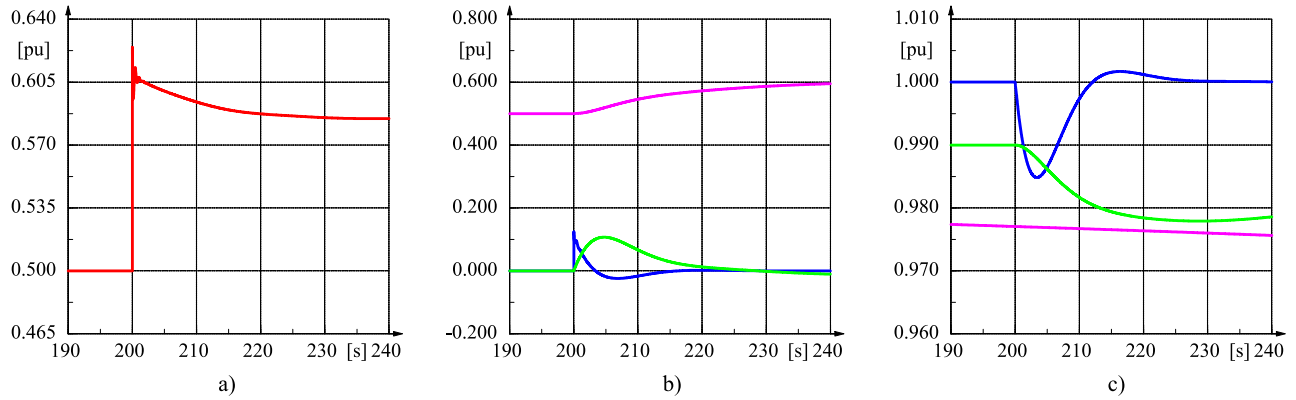

Figure 6 a) Increase in power output, b) Current flow from the SPP storages and c) Voltage levels of the storages during the long time frame

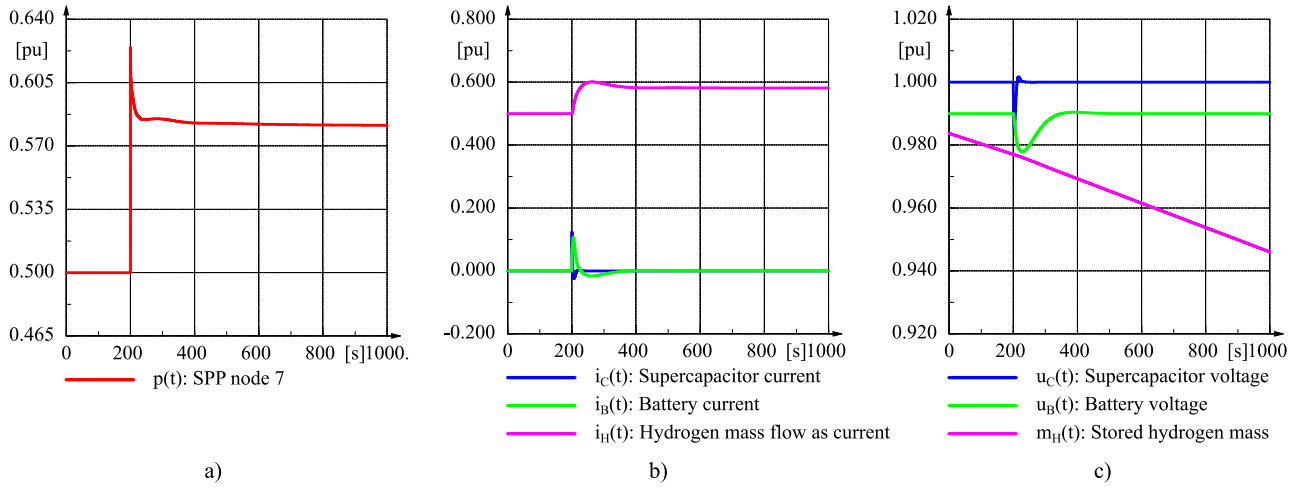

Figure 7 a) Increase in power output, b) Current flow from the SPP storages and c) Voltage levels of the storages during the long time frame

peak output since the rate of change of frequency at node 7 is higher than in node 12 or 19. Due to the lower electrical distance between the nodes 12 and 13 than that between nodes 13 and 19, the hydroelectric power plant (HPP) at node 12 experiences a higher rate of frequency change and provides a greater inertial response than the TPP.

This is more evident in Fig. 4b which displays the supplying of primary control power by the different power plants. The power output of the HPP and TPP continues to rise steadily with the HPP showing a greater rate of increase. Meanwhile the output of the SPP decreases steadily so that the overall increase in power generation balances the increase in power demand. Fig. 4c demonstrates the secondary control power flows illustrating that the power output of the SPP and TPP levels off at the same value. This is because all three power plants have the same time con-

ISBN 978-3-8007-5081-8

stant magnitudes for their secondary controller. However, the HPP has a slightly lower power output owing to the friction on its penstock walls.

Next, the behavior of the internal components of the SPP at node 7 is investigated to examine the power plant's ability to provide ancillary services. Fig. 5a shows the active power output of the SPP at node 7. Fig. 5b illustrates the currents out of the respective storages while Fig. 5c exhibits the resulting change in the voltage or mass levels of these three storages. These trends are presented in three different time scales in Fig. 5-7, in order to highlight the regulating services provided by the SPP and the storages associated with each of the control powers.

4.1.1 SPP Short Time Frame Response

The graph in Fig. 5b shows that, like rotating masses in a TPP, the supercapacitor immediately starts to supply inertial power with the onset of the positive disturbance, so the SPP can meet the increased network demand. As a result, the supercapacitor voltage decreases. To ensure that the supercapacitor is able to respond to further disturbances, the DC-DC converter between the supercapacitor and battery takes over supplying the disturbed network demand and subsequently recharges the supercapacitor to its nominal value, as shown in Fig. 6c. The recharging phase of the supercapacitor is visible in Fig. 6b for the time duration when the supercapacitor current is negative.

4.1.2 SPP Medium Time Frame Response

For this primary control, the DC-DC converter only uses the energy stored in the battery. Therefore, the battery current increases and its voltage decreases, as shown in Fig. 6b and c. In addition, the DC-DC converter limits the battery current gradient to lower the stress on the storage device and in the process improves its lifetime.

The battery voltage operates within a defined voltage dead band under steady state conditions. When the battery voltage surpasses the lower threshold of 0.99 pu in Fig. 6c, the DC-DC converter on the upper branch between the battery and the fuel cell in Fig. 2, increases its power flow to the grid. This continues until it fully supplies the disturbed network demand on its own. Furthermore, the converter recharges the battery and raises its voltage to be within permissible limits of the dead band. It is able to perform these functions since it controls its adjacent fuel cell. As a result, it increases the power supplied from the fuel cell, according to the required power demand of the grid. This supply of secondary control power can be seen in the form of increased hydrogen mass flow in Fig. 6b.

4.1.3 SPP Long Time Frame Response

In the longer time frame represented in Fig. 7c, the consequent decrease in the stored hydrogen mass is shown. During steady state operation the network demand is fully supplied by the hydrogen storage alone. The supercapacitor and battery currents return to zero and their voltage levels are also restored to the respective initial values. The SPP continues to output a constant active power owing to the steady rate of hydrogen mass flow, as shown in Fig. 7a and b. However, the SPP is not only able to supply power to the grid, like a CPP, but can also store it. This is clarified in greater detail in the following investigation.

4.2 Case II

This case study involves examining the dynamic behavior of the power plants in the 25 node network in a more futuristic scenario. To depict such a situation, the coal fired TPP in node 19 of Fig. 1 is switched off since it is expected that such power plants will not be a part of the electrical grid anymore due to the exhaustion of fossil fuel reserves. Consequently, the loadflow values for this investigation are slightly altered. Each of the 14 loads in the grid now consumes 2 MW of active power. The total consumption of 28 MW is balanced by the HPP, generating 10 MW and the combination of five SPPs and four WPPs each producing 2 MW of active power. The base power value of the per-unit system is still 10 MVA.

Next, a ramp is applied to the power generation of the four WPPs between the time duration of 200 s to 800 s. This portrays a situation when the power output of the WPPs would increase steadily due to an increase in the wind speed. As a result, the output of each WPP increases from 2 MW to 10 MW, shown as pu values in Fig. 9a. At the same time, the power output of the SPP and HPP decreases to maintain the balance between generation and demand. The output of the HPP levels off at 5 MW (0.5 pu) since it should function at least at 50% of its nominal power to maintain feasible operation. This is compensated by the five SPPs which then start to reduce their power output at a faster rate. Such values are chosen for the WPP output ramp so that the power output of every SPP reduces beyond zero and its energy storing ability can be studied. Due to this increase in power generation the grid frequency rises steadily, reaching its peak value when the ramp ends as shown in Fig. 8. After this time, the secondary controllers of the power plants take over significantly and return the frequency to its initial value of 1 pu.

Fig. 9a depicts that as soon as the ramp in WPP generation starts, the HPP and SPP outputs decrease. The reduction in the SPP power production consequently causes the output of the DC-DC converter, between the supercapacitor and battery, to decrease as well. At this time, the hydrogen mass flow from the SPP fuel cell is higher than the output of this DC-DC converter. The resulting difference leads to a surplus power flow which charges the battery, signified by the first short negative dip in battery current in Fig. 9b. The corresponding battery voltage, displayed in Fig. 9c, increases beyond the lower threshold of 0.99 pu. This causes the DC-DC converter controlling the fuel cell to gradually reduce the fuel cell output to zero.

Once the output power of the SPP becomes negative, the battery is once again charged by the grid side DC-DC converter due to excess power arriving from the grid. Accordingly, the battery voltage rises. Once the voltage crosses its upper threshold of 1.01 pu, the DC-DC converter regulating the electrolyzer increases the converter output, gradually raising the hydrogen mass flow rate towards the hydrogen storage and subsequently increasing the stored mass.

ISBN 978-3-8007-5081-8

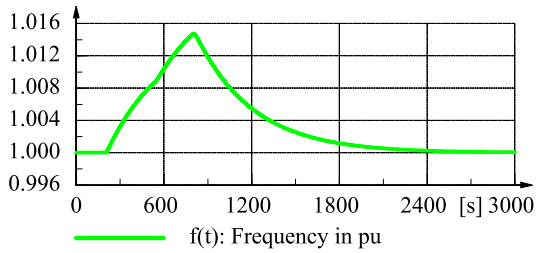

Figure 8 Change in grid frequency due to the ramp in the power generation by the WPPs

When the ramp ends at 800 s, both the capacitor and battery are discharged by the regulating DC-DC converters to retain their voltage levels of 1 pu and 1.01 pu respectively. From then onwards, the power storage of the SPP is only governed by its steady rate of hydrogen mass flow.

5 Conclusion

This paper exhibited the ability of SPPs to function effectively with CPPs and RES in a 25 node frequency controlled grid. Inside this network, a disturbance was created initially by applying a step increase in the the load consumption and then a ramp to increase the WPP generation. The corresponding dynamic responses of the CPPs, WPPs and SPPs were investigated. It was shown that while supplying or storing power as a result of the disturbance, a SPP is able to provide the necessary ancillary response in the form of inertial, primary and secondary control. These power flows inside the SPP are regulated by the respective DC-DC converters between these storages. Currently, studies involving the subtransient and transient behavior of SPPs during short circuit faults are underway. The reactive power control schemes of the SPPs are also being investigated. In addition, further research will be required to estimate the total losses as well as the market compatibility of this novel system and hence prepare a quantitative comparative study in relation to the current power system.

6 Literature

[1] World Energy Balances IEA (2016), Total Final Consumption (TFC) by source Germany 1990 - 2016.

[2] Weber, H., Hamacher, T., and Haase, T. (2006) Influence of wind energy on the power station park and the grid. *IFAC Proceedings Volumes*, **39**, 59–64.

[3] Vgb PowerTech (2018), Electricity Generation Facts and Figures 2018|2019.

[4] Energiewende (2015), The Energy of the Future, fifth energy transition monitoring report.

[5] Liang, X. (2016) Emerging power quality challenges due to integration of renewable energy sources. *IEEE Transactions on Industry Applications*, **53**, 855–866.

[6] German Institute for Economic Research (2019) *Phasing out Coal in the German Energy Sector*. DIW Berlin.

[7] Hadjipaschalis, I., Poullikkas, A., and Efthimiou, V. (2009) Overview of current and future energy storage technologies for electric power applications. *Renewable and sustainable energy reviews*, **13**, 1513–1522.

[8] Dunn, B., Kamath, H., and Tarascon, J.-M. (2011) Electrical energy storage for the grid: a battery of choices. *Science*, **334**, 928–935.

[9] Weber, H., Ahmed, N., and Baskar, P. (2018) Nodal voltage angle control of power systems with renewable sources, storages and power electronic converters. *2018 International Conference on Smart Energy Systems and Technologies (SEST)*, pp. 1–6, IEEE.

[10] Weber, H., Ahmed, N., and Baskar, P. (2018) Power re-dispatch reduction with nodal voltage angle control in electrical energy supply systems. *IFAC-PapersOnLine*, **51**, 576–581.

[11] Teichmann, D., Arlt, W., Wasserscheid, P., and Freymann, R. (2011) A future energy supply based on liquid organic hydrogen carriers (LOHC). *Energy & Environmental Science*, **4**, 2767–2773.

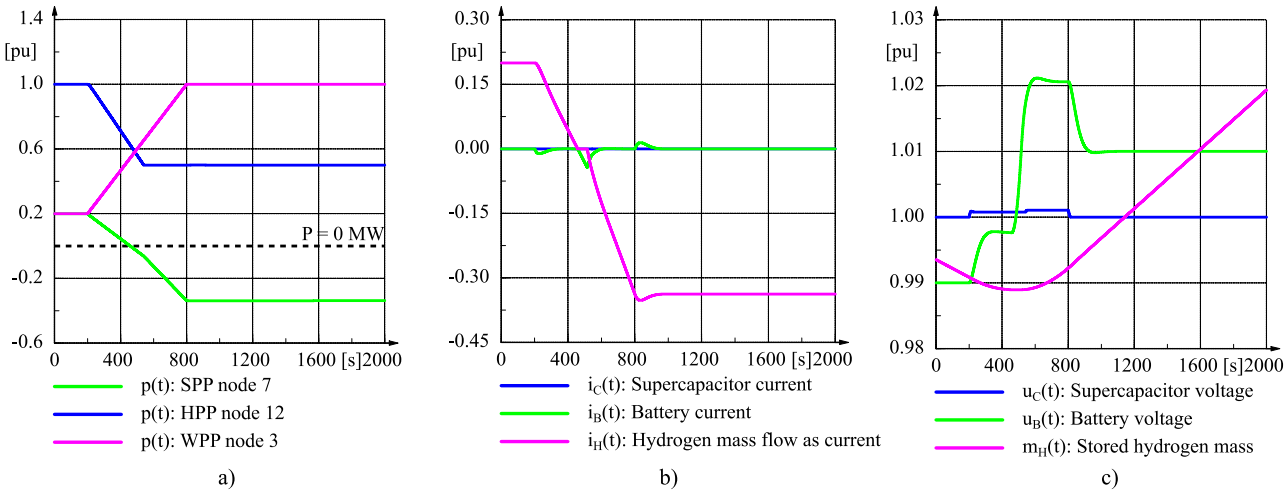

Figure 9 a) Change in active power output of the three different types of power plants, b) Current from from the SPP storages and c) Voltage levels of the storages during the long time frame

ISBN 978-3-8007-5081-8